Chemical Science

Accepted Manuscript

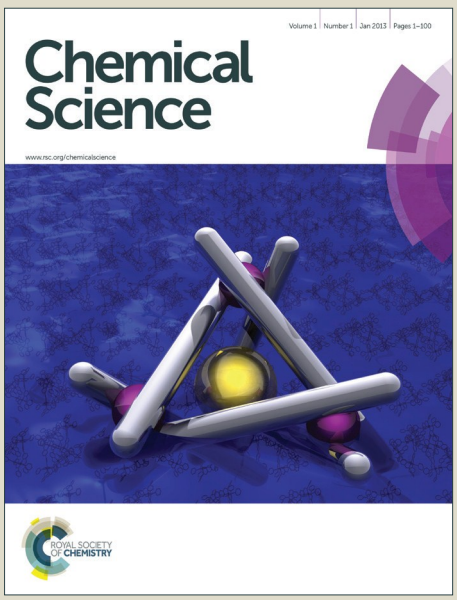

ROYAL SOCIETY OF CHEMISTRY

www.rsc.org/chemicalscience

Journal Name

ARTICLE

Insight into the Charge Transfer in Particulate Ta_3N_5 Photoanode with High Photoelectrochemical Performance†

Received 00th January 20xx,
Accepted 00th January 20xx

DOI: 10.1039/x0xx00000x

www.rsc.org/

Zhiliang Wang,‡[ab] Yu Qi,‡[ab] Chunmei Ding,[a] Dayong Fan,[ab] Guiji Liu,[ab] Yongle Zhao[ab] and Can Li[a*]

Charge separation is one of the most critical factors for generating solar fuels via photoelectrochemical water splitting, but it is still not well understood. This work reveals the fundamental role of charge transfer in photoanodes for achieving high charge separation efficiency. Specially, we fabricate particulate Ta_3N_5 photoanode in a bottom-up method. By improving the charge separation with refined necking treatment, the photocurrent is increased by two orders of magnitude. The charge separation efficiency (η_{sep}) is analyzed by dividing it into charge generation efficiency (Φ_{gene}) and transportation efficiency (Φ_{trans}). And necking treatment is found to improve the electron transfer prominently. And transient photovoltage (TPV) based on Dember effect is firstly used to confirm the benefit of necking treatment in improving the charge transportation. The superior electron transfer in necked-Ta_3N_5 electrode is further evidenced by the facile electron exchange reaction with the ferri/ferrocyanide redox couple. Moreover, cobalt phosphate is found to promote both charge separation and surface reaction, resulting in a photocurrent of 6.1 mA/cm^2 at 1.23 V vs RHE, which is the highest response for particulate photoanode.

Introduction

Photo-induced water splitting paves a promising way for the production of renewable solar fuels by converting solar energy to hydrogen directly. To achieve this conversion process, photocatalysis (PC) and photoelectrocatalysis (PEC) are technological choices.[1-4] Many kinds of materials have showed photoresponse in PC but failed in PEC due to the issue of electrodes fabrication.[2, 5, 6]

In PC, an efficient charge separation in particles can usually lead to fast reaction at the semiconductor/liquid interface with the assistance of suitable cocatalyst.[7] In PEC, however, photogenerated electrons must transfer through the film and be collected by the substrate to match the surface reaction. Thus, the charge transportation in the films also plays a fundamental role in the whole PEC process.[8] And the interfaces of particle-particle (PP) and particle-substrate (PS) are critically important for charge transportation. To ensure well connections at these interfaces, semiconductor is usually epitaxially grown on a conductive layer in-situ by, for instance, hydrothermal,[9] chemical bath,[10] and vapour deposition.[11, 12] And electrodes in low dimensional structure[13, 14] or host-guest structure[15, 16] are intentionally designed to improve the charge transportation efficiency in the electrode so as to decrease the electron-hole recombination. However, most previous researches focus on charge transfer in the semiconductor particles since it determines the generation of separated electron-hole pairs,[17-19] little attention has been paid on clarifying the charge transfer process in the film which also plays a determinable role during the photoelectrochemical reaction.

Transient photovoltage (TPV) can provide direct insight into the charge transfer process through the electrode. Upon illumination, Dember photovoltage is generated.[20] It stems from the diffusion difference of photogenerated electrons and holes. Typically, the gradient distributed light in the film excites photogenerated electron-hole pairs in gradient concentration[21, 22] which will cause them diffusing from high concentration region (surface, high light intensity) to the low region (bulk, low light intensity) at different velocity. Then the electron-hole pairs drift apart and electric filed builds up. The decay process of the photovoltage can reveal the charge transfer process in the film.

Cyclic voltammetry (CV) in darkness can also reveal the electron transfer in electrodes.[23] For the cathodic reaction, electrons must transfer through the films before exchanging with efficient redox couple, *e.g.* $Fe(CN)_6^{3-}/Fe(CN)_6^{4-}$. The magnitude of cathodic current and potential of the reduction peak can reveal the electron transportation in the film. In addition, particulate electrode with well-connected film can result in porous structure which provides large electrochemical surface area for reaction. And the area is proportional to the capacitance of Helmholtz layer which can be determined from

[a] State Key Laboratory of Catalysis, Dalian Institute of Chemical Physics, Chinese Academy of Sciences, Dalian National Laboratory for Clean Energy, The Collaborative Innovation Center of Chemistry for Energy Materials (iChEM), Zhongshan Road 457, Dalian, 116023, China. E-mail: canli@dicp.ac.cn
[b] University of the Chinese Academy of Sciences, Beijing, 100049, China.
†Electronic Supplementary Information (ESI) available. See DOI: 10.1039/x0xx00000x
‡ These authors contribute equally to this work.

CV.[24] Thus we can evaluate the charge transportation in the film in electrochemical method.

Suitable material and fabrication method of the electrodes are important for us to pinpoint the issue of charge transportation. For material, semiconductor with long free path is the best candidate because it permits us to focus on the charge transfer at the PP interfaces regardless of the charge diffusion in the semiconductor crystals. Ta_3N_5 is reported to have a diffusion length of ~10^3 nm,[25] indicating a long life time of photogenerated charges. Moreover, Ta_3N_5 has showed an outperformed photocatalytic oxygen evolution activity,[26] indicating an effective charge separation in the Ta_3N_5 crystals. And the excellent light harvest ability of Ta_3N_5 makes it an appealing material for photoelectrochemical water splitting with a potential solar energy conversion efficiency of 15 % under AM 1.5 G sunlight.[27] For the fabrication of electrode, a bottom-up method, that is by depositing as-prepared semiconductor particles on the conductive substrate to form a particulate electrode, can make it more facial to regulate the charge transfer at the PP and PS interfaces without influencing the intrinsic properties of the semiconductor such as the light absorption, carrier concentration *etc*. Electrophoretic deposition (EPD) method is an alternative choice. A wide range of semiconductors can be fabricated into electrodes with controllable thickness by EPD, such as Fe_2O_3,[28] $BiVO_4$,[29] Ta_3N_5,[30] TaON.[31-32] And the post necking treatment has been found to be powerful in improving the PEC response.[30-34] Some explanation to the possible function of necking treatment has been proposed,[31] but more stringent evidences are appealed to identify it.

Herein, we take Ta_3N_5 as a demonstration to show the influence of charge transportation on the PEC performance of particulate Ta_3N_5 electrode. By optimizing the substrate, precursor concentration, temperature of necking treatment and cocatalyst loading, we achieve the highest photocurrent for electrodes fabricated by EPD. The TPV based on Dember photovoltage and CV measurements are used to clarify the critical effect of necking treatment on charge transfer at the interfaces of particle-particle and particle-substrate.

Experimental

Ta_3N_5 powder synthesis Ta_2O_5 powder (Amresco Chemical, ≥99.99%) was immersed in water. Then it was dried and annealed in air at 800 ^oC for 2 h, then nitridized in ammonia flow (250 sccm) at 950 ^oC for 15 h.

Ta_3N_5 electrode fabrication The as-synthesized Ta_3N_5 powder (50 mg) was dispersed into 50 mL acetone (Kemeol, ≥99.5%) under ultra-sonic for 10 min. Then 20 mg iodine was dissolved into the suspension to make it suitable for EPD. Ti foil (1 cm × 2 cm) was used as substrate after totally washed in 1 M HF aqueous, pure water and anhydrous ethanol. A piece of fluorine doped tin oxide (FTO, Nippon Glass Sheet) glass (2 cm × 3 cm) is used as counter electrode with the conductive layer facing to Ti foil at a distance of 1 cm. The Ta_3N_5 crystal was deposited to the Ti foil at a bias of 20 V for 1 min.

Necking treatment 20 mM $TaCl_5$ (Alfa Aesar, ≥99.99%) was dissolved into anhydrous methanol (Sinopharm Chemical Reagent, ≥99.5%). 10 μL $TaCl_5$ solution was then dropped onto the raw Ta_3N_5 electrode (denoted as raw-Ta_3N_5, area of 1~1.3 cm^2) for 5 times (50 μL in total) to form the $TaCl_5$ treated Ta_3N_5 electrode (denoted as $TaCl_5$-Ta_3N_5 electrode) based on Ref. 40. Then the $TaCl_5$-Ta_3N_5 electrode was calcinated at 600 ^oC (5 ^oC/min) for 60 min under NH_3 flow (100 sccm), and the as-prepared electrode is donated as necked-Ta_3N_5. For comparison, the raw-Ta_3N_5 electrode was also heated in the same way without $TaCl_5$ solution (denoted as heated-Ta_3N_5).

Cobalt phosphate deposition 5 mM $Co(NO_3)_2$ (Sinopharm Chemical Reagent, ≥99.0%) was dissolved into 0.5 M NaPi buffer solution (pH 6.8). Then CoPi was electrochemically deposited onto Ta_3N_5 electrode under simulated light (AM 1.5 G, 100 mW/cm^2) illumination at current density of 10 μA/cm^2.

Characterization The absorption spectra from 350 nm to 800 nm were taken on Cary 5000 UV-VIS-NIR spectrophotometer (JASCAO) equipped with an integrated sphere. X-ray diffraction (XRD) patterns were recorded on Rigaku D/Max-2500/PC powder diffractometer operating at 40 kV and 200 mA with Cu Kα radiation (λ= 0.154 nm) at a scanning rate of 5^o/min. The morphology of the electrodes was imaged by Quanta 200 FEG scanning electron microscope (SEM). High-resolution transmission electron microscopy (HRTEM) images were obtained on Tecnai G2 F30 S-Twin (FEI Company) with an accelerating voltage of 300 kV. X-ray photoelectron spectroscopy (XPS) was recorded on VG ESCALAB MK2 spectrometer with a monochromatic Al Kα radiation (12.0 kV, 240 W). All the bonding energy was corrected in reference to the C 1s (284.8 eV).

Transient photovoltage measurement

The transient photovoltage (TPV) was measured with pulsed laser (355 nm, 5 ns) using a Ta_3N_5 device (see ESI for detail). The average power was 122 mW unless otherwise mentioned. The signals were read from an oscilloscope (Tektronix TDS 3012C).

(Photo)electrochemistry measurement

The cyclic voltammetry was measured without illumination in the electrolyte of 1 M NaOH or NaOH (1 M) +$K_3Fe(CN)_6$ (0.25 M) aqueous solution at the scan rate of 100 mV/s in the range of -1.4 V~ 0.4 V vs SCE. For the electrochemical area measurement, the scan rate varied from 20 to 500 mV/s in the range of -0.1 V~ 0.2 V vs SCE in 1 M NaOH aqueous solution.

The photocurrent was recorded under simulated light (AM 1.5 G, 100 mW/cm^2) at a scan rate of 50 mV/s from -0.8 V to 0.6 V vs SCE in 1 M NaOH aqueous solution (pH 13.6).

The incident photon-to-current conversion efficiency (IPCE) was measured under monochromatic light irradiation provided by a tungsten lamp equipped with monochromator (CROWNTECH, QEM24-D 1/4 m Double).

Faradaic efficiency was tested by recording the photocurrent and the generated O_2 simultaneously. The O_2 evolution was evaluated by gas chromatography (GC, Agilent 7890a GC) with a 5 Å molecular sieve column. Argon carrier gas with a velocity of 10.0 ml/min was used to purge the working electrode compartment to carry the evolved gases to GC for analysis.

The quantity and retention time of the gases were calibrated with a series of standard gas samples.

All the (photo)electrochemical tests were conducted on Ivium Potentiostat/Galvanostat in a 3-electrode system with a quartz window. A piece of platinum foil (2 cm×2 cm) was used as counter electrode and saturated calomel electrode (SCE, 0.241 V vs RHE) as the reference electrode. The potential was transferred to the reversible hydrogen electrode (RHE) scale by Nernst equation as bellow:

$$E(RHE)=E(SCE)+ 0.059*pH +0.241 \quad (1)$$

Results and discussion

The morphology of the electrodes was first characterized by SEM. The SEM image of cross-section view shows that the as-prepared electrode has a thickness of 5~7 μm (Figure S1). And the top-view images show that the surface of porous raw Ta_3N_5 (Figure 1a) is covered with an amorphous layer after treating with $TaCl_5$ solution (Figure 1b). The following heat treatment seems to retrieve the smooth surface of Ta_3N_5 but boundaries between particles become dim compared to those on raw-Ta_3N_5 electrode (Figure 1c). HRTEM image confirms the existence of 1~5 nm amorphous layer (Figure 1d). This amorphous tantalum species may bridge the adjacent Ta_3N_5 particles. The XRD patterns (Figure S2) show no change of the Ta_3N_5 crystal with necking treatment. But the surface change was revealed in XPS spectra (Figure 1e). There is no prominent difference between raw-Ta_3N_5 and heated-Ta_3N_5 electrodes. But for $TaCl_5$-Ta_3N_5 electrode, another peak at 28.1 eV was observed, in agreement with the reported Ta $4f_{5/2}$ in tantalum oxide.[35-36] It is inferred that the amorphous layer in Figure 1b may be tantalum oxide. Since it was covered on the raw-Ta_3N_5 electrode, the intensity of O 1s (530.7 eV) became stronger, and the intensity of Ta $4f_{7/2}$ (24.6 eV) became weaker after treating with $TaCl_5$ solution, indicating the screening effect of the amorphous tantalum oxide. And it is also inferred that Ta $4f_{7/2}$ at 24.6 eV is stemmed from Ta-N bonds. After necking treatment, the intensity of O 1s (530.7 eV) ascribed to surface absorbed oxygen species is prominently decreased compared to $TaCl_5$-Ta_3N_5 electrode. And the Ta $4f_{5/2}$ ascribed to Ta-O is shifted from 28.0 eV to 27.6 eV, and Ta $4f_{7/2}$ ascribed to Ta-N bond shifted from 24.6 to 25.0 eV for necked-Ta_3N_5 electrode. It is suggested that a nitrogen doped tantalum layer has been formed. Because Ta-N bond is more covalent than Ta-O bond, nitrogen doping of tantalum oxide during necking treatment will shift the binding energy of Ta 4f to low energy.[36-38]

Albeit the little changes of the morphology of Ta_3N_5 particles, the PEC performance shows great difference with necking treatment (Figure 2a). The raw-Ta_3N_5 electrode exhibits notoriously low photoresponse, and so does the $TaCl_5$ treated electrode. But after necking treatment, the photocurrent of necked-Ta_3N_5 electrode increases to 1.56 mA/cm^2 from 9 μA/cm^2. For the necking treatment, the $TaCl_5$ concentration and post heating temperature have great influence on the photoresponse of necked-Ta_3N_5 electrode (Figure S3). And the optimized $TaCl_5$ concentration is 15~20 mM (concentration at 20 mM gives the best repeatability) and the temperature is

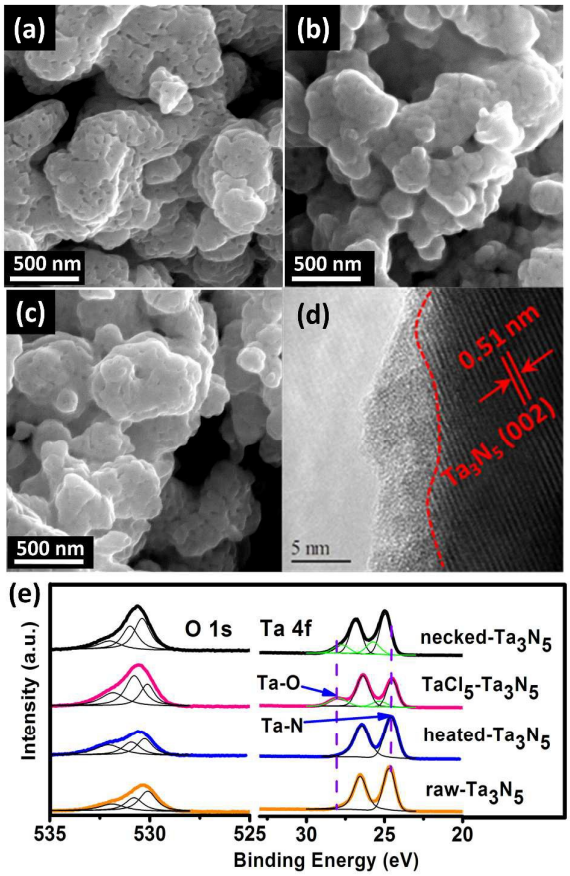

Figure 1. SEM images of (a) raw-Ta_3N_5 electrode, (b) $TaCl_5$-Ta_3N_5 electrode, and (c) necked-Ta_3N_5 electrode. (d) HRTEM image of necked-Ta_3N_5 electrode. (e) XPS spectra of O 1s and Ta 4f for raw-Ta_3N_5 (orange), heated-Ta_3N_5 (blue), $TaCl_5$-Ta_3N_5 (pink), and necked-Ta_3N_5 (black) electrodes.

600 °C for the refined necking treatment. At high temperature, the particles will have strong connection with each other at the PP and PS interfaces. However, NH_3 has strong capability of reduction at high temperature. It can damage the normally used FTO substrate.[28, 31] Some metal based candidates were chosen and Ti foil gave better result (Figure S4). The benefit of

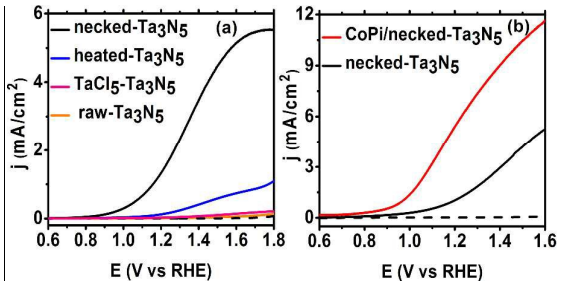

Figure 2. Current-potential (j-E) curves of (a) raw-Ta_3N_5 (orange), $TaCl_5$-Ta_3N_5 (pink), heated-Ta_3N_5 (blue), necked-Ta_3N_5 (black), and (b) CoPi/necked-Ta_3N_5 (red) electrode. Electrolyte: 1 M NaOH aqueous solution. Illumination: 100 mW/cm^2, AM 1.5 G.

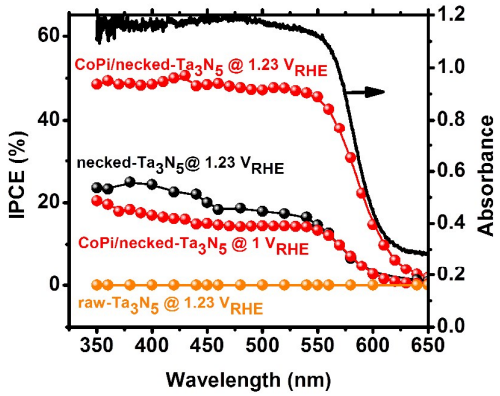

Figure 3. IPCE of raw-Ta_3N_5 (orange), necked-Ta_3N_5 (black), and CoPi/necked-Ta_3N_5 (red) electrodes. The absorption spectrum (black solid curve) for raw Ta_3N_5 is presented for comparison.

calcination is also confirmed by the improved photoresponse of heated-Ta_3N_5 compared to raw-Ta_3N_5 electrode. Further cocatalyst loading, e.g. CoPi,[39] on necked-Ta_3N_5 electrode efficiently accelerates the water oxidation to an optimized current of 6.1 mA/cm^2 at 1.23 V vs RHE (Figure 2b), which is higher than most reported results fabricated by EPD method.[30, 31, 40, 41] In Figure 3, IPCE action spectra show the quantum efficiency at different irradiation wavelength, which are in agreement with the absorption of Ta_3N_5. The raw-Ta_3N_5 electrode shows very low IPCE, but after the refined necking treatment, it dramatically increases to more than 20 %. And the IPCE is much higher by loading CoPi or increasing bias to accelerate the consumption of photogenerated charges.

The refined necking treatment plays a key role in boosting the photoanodic performance of the particulate Ta_3N_5 electrode. And it is also essential for the cocatalyst functioned Ta_3N_5 photoanode. Thus we endeavour to pinpoint the exact role of necking treatment by analysing the reaction at the semiconductor/liquid interface and charge transfer at PP and PS interfaces on the particulate Ta_3N_5 electrode.

As for electrode made from powder, necking treatment may have influence on both the intrinsic property of Ta_3N_5 particles and the connection among particles. In order to peep at the possible change of Ta_3N_5 crystals, the absorption spectra and photocatalytic activity (see ESI for detail) were measured. The absorption spectrum of Ta_3N_5 has little change after necking treatment (Figure S5 a), indicating that the necking treatment does not influence the intrinsic light harvest in Ta_3N_5. And from the absorption spectra, the marginal photocurrent of the electrode was evaluated to be ~12.6 mA/cm^2 under simulated sunlight (AM 1.5 G, 1 sun) (Figure S5). The influence of necking treatment to the Ta_3N_5 particles were further verified by photocatalytic O_2 evoltuion. In a PC reaction (Figure 4a), light is harvested in Ta_3N_5 crystal. Then the photogenerated charges drift to the active sites to take part in the surface reaction. The proportion of photogenerated charges that reach the surface reaction sites to those generated in Ta_3N_5 particles upon illumination is referred as charge generation efficiency (Φ_{gene}), which is basically the charge separation efficiency in Ta_3N_5 crystal. To preventing the confusing the separation efficiency in electrode as it will be mentioned below, we define it as generation efficiency for crystal. And the generation efficiency is largely determined by the bulk property of the crystal. The proportion of photogenerated holes that take part in the (electro)chemical reaction to those arrived at the reaction sites is referred as injection efficiency (η_{inj}), which is influenced by the surface property of Ta_3N_5. When the surface is not preferred for catalytic water oxidation, although sufficient holes reach the reaction sites, they cannot be consumed in time and the η_{inj} will be less than unit. In the presence of efficient electron scavengers, the influence of electron in the crystal is limited and the PC reaction can be used to evaluate the intrinsic properties of the Ta_3N_5 particles, such as the charge generation in the crystals and holes injection on the surfaces.[42] The PC activities of the Ta_3N_5 powder from raw-Ta_3N_5 electrode and necked-Ta_3N_5 electrode were evaluated with $AgNO_3$ as sacrifice.[26] As it is shown in Figure 4b, the amount of released O_2 for necked-Ta_3N_5 has slightly decrease, implying that necking treatment has limited influence to the intrinsic property of Ta_3N_5.

Then we focus on the impact of necking treatment to the electron transfer at the PP and PS interfaces in Ta_3N_5 electrode. In a PEC reaction (Figure 4a), electrons and holes should be considered simultaneously since the electrons need

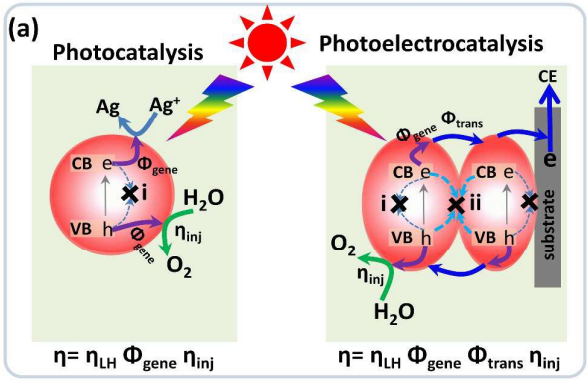

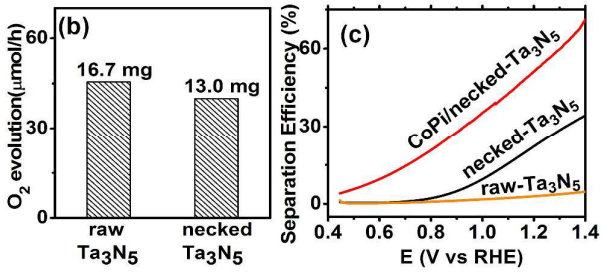

Figure 4. (a) The schematic comparison O_2 evolution processes via photocatalysis ($AgNO_3$ as electron scavenger) and photoelectrocatalysis. (b) Photocatalytic activity of the Ta_3N_5 powder peeled from raw-Ta_3N_5 and necked-Ta_3N_5 electrodes. The mass of the photocatalyst is list above the column respectively. (c) Charge separation efficiency of raw-Ta_3N_5 (orange), necked-Ta_3N_5 (black), and CoPi/necked-Ta_3N_5 electrodes (red).

to transfer through the Ta_3N_5 films during the PEC water oxidation. The transportation of photogenerated charges will be another factor that limits the PEC performance.

As it is reported, the final photocurrent is determined by the following expression:[43, 44]

$$J=J_o*\eta_{LH}*\eta_{sep}*\eta_{inj} \quad (2)$$

Where J_0 is the theoretical photocurrent, η_{LH} is the light harvest efficiency, η_{inj} is the charge injection efficiency as defined above and η_{sep} is separation efficiency in the electrode as defined in Ref. 43.

The absorption and PC water oxidation measurement have revealed that necking treatment has little influence on light harvest (η_{LH}) and surface reaction (η_{inj}). Hence, the difference of charge separation (η_{sep}) of the electrode should take responsibility for the huge difference of the PEC activity. Taking H_2O_2 as hole scavenger,[43] the charge separation efficiency is calculated. In Figure 4c, it reveals that the charge separation in raw-Ta_3N_5 electrode is inefficient, but necking treatment improves η_{sep} to more than 30 % at the bias of 1.3 V vs RHE. Interestingly, we found that CoPi/necked-Ta_3N_5 electrode has an even higher η_{sep} of 60 % at 1.3 V vs RHE.

The higher separation efficiency, in other words, means less electron-hole recombination in the electrode. For photoelectrocatalytic reaction occurred on particulate electrode (Figure 4a), the recombination may occur in two routes: (i) recombination in the particles through, for example, bulk defects or surface states; (ii) recombination at the interfaces of particles. Thus the measured separation efficiency should be dependent on the charge generation in particles and transfer among particles under illumination:

$$\eta_{sep}=\Phi_{gene}\cdot\Phi_{trans} \quad (3)$$

Where Φ_{gene} is the charge generation efficiency as mentioned in Ta_3N_5 crystal, relating to recombination process (i), and Φ_{trans} is the transportation efficiency for photogenerated charges transferring through PP and PS interfaces before arriving at the conductive substrate from the birthplace,[45] relating to recombination process (ii).

CoPi has been reported to suppress the surface states, and more long-lived photogenerated holes can survive in the particles.[46] Thus, the Φ_{gene} is increased and this leads to the cocatalyst promoted charge separation for CoPi/necked-Ta_3N_5 electrode (Figure 4c). For the necked-Ta_3N_5 electrode, the previous absorption (Figure S5) and PC activity (Figure 4b) indicates a similar Φ_{gene}. Thus, the dramatically improved η_{sep} for necked-Ta_3N_5 electrode should stem from the improved Φ_{trans} by necking treatment.

To consolidate the conclusion, prototypical devices fabricated from Ta_3N_5 electrodes (Figure 5a, See ESI for detail) were used to delve into the charge transportation in the electrode by TPV. In Figure 5b, the necked-Ta_3N_5 based device shows higher transient photovoltage and faster decay process than the raw-Ta_3N_5 based device does. A linear response of current-bias (Figure S6) confirms the Ohmic contact at the interfaces of PS.[20] Thus, the detected photovoltage plausibly stems from the Dember effect. And it was further confirmed by the relationship between the direction of induced laser and electric field. For Dember effect, holes always stay closer to the top layer, the direction of the electric filed is always consistent with the direction of the laser beam (Figure S7 a). And the intensity of Dember voltage is determined by the amount of separated charges. Light in stronger intensity will induce more separated charges, hence higher photovoltage (Figure S7 b). When the intensity of the induced light is the same, that is the same amount of charges will be generated, the higher photovoltage can necessarily mean better charge separation. Thus the higher photovoltage of necked-Ta_3N_5 device indicates that it has better charge separation which is in accordance with the result in Figure 4.

When light is shadowed, the electron-hole pairs will recombine reversely, leading to the dynamical decay of Dember photovoltage at the time scale of μs (Figure 5b, solid line). Two plausible recombination processes mentioned above are

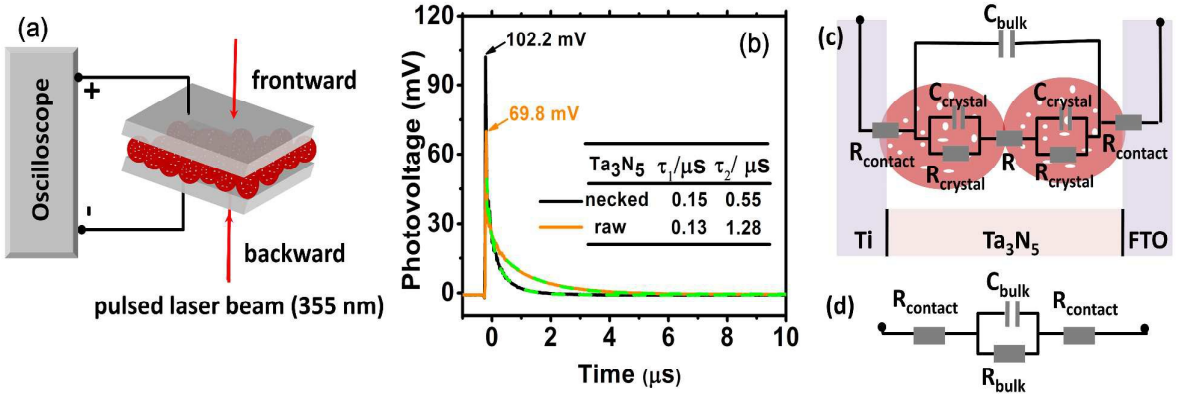

Figure 5. (a) Schematic setup for TPV test. (b) TPV spectra of raw-Ta_3N_5 (orange) and necked-Ta_3N_5 electrode (black) with dual exponential fitted curves (green dashed curves). The inserted table shows the life times of the two electrodes, respectively. (c) Equivalent circuit of the device. (d) The simplified circuit of (c). $R_{contact}$ is the serial resistance at the particle-substrate interfaces; R_{bulk} is the total resistance in Ta_3N_5 films including the resistance in Ta_3N_5 particles ($R_{crystal}$) and at particle-particle interfaces (R); C_{bulk} is the capacity of the parallel-plate capacitor built by Ti and FTO.

involved in the decay process. And the former process is usually faster. A dual exponential fitness (Figure 5b, dashed line) gives delicate description to the curves with a fast decay process (recombination in Ta_3N_5 crystals, life time of τ_1) and a slow one (recombination at the interfaces, life time of τ_2). The two electrodes have approximate τ_1, confirming again that the Ta_3N_5 particles on both electrodes have similar charge generation efficiency (Φ_{gene}) as PC result reveals in Figure 4a. And the necked-Ta_3N_5 electrode has lower τ_2, indicating that the electron-hole pairs are more facile to recombine through the interfaces in the TPV devices.

In order to clarify the result of TPV further, an equivalent circuit (EC) based on transmission line model[47] (Figure 5c) is used to simulate the decay process in the device. Because there is no semiconductor/electrolyte interface, only three processes are considered: (i) the electron transport resistance in the Ta_3N_5 crystals ($R_{crystal}$), (ii) the electron transport resistance among particles (R) and particles-substrate ($R_{contect}$), (iii) a capacitive charging to the porous Ta_3N_5 matrix (C_{bulk}). For the Ta_3N_5 crystal, the conduction band or the defect energy level can accommodate electrons which can behave like a capacity ($C_{crystal}$). And C_{bulk} can be estimated to be at the order of 10^{-5} F/cm^2, while $C_{crystal}$ to be 10^{-8} F/cm^2 (see ESI for detail). Thus, the $C_{crystal}$ is much smaller compared to the C_{bulk} and the series of $C_{crystal}$ make it even smaller that we can ignore $C_{crystal}$. So the equivalent circuit in Figure 5c can be reduced to that in Figure 5d, including the resistance among and in Ta_3N_5 particles. And the time constant ($\tau`=R_{bulk}\cdot C_{bulk}$) of electronic decay in the simulated circuit corresponds to the life time (τ) determined by TPV. For the bulk capacitance (C_{bulk}) of the two devices (raw-Ta_3N_5 and necked-Ta_3N_5), they are estimated to be at the same order of magnitude based on eq. S1 (ESI). Hence, the change in time constant can reflect the change of resistance in the device. Comparing the life time of τ_2 in two kinds of Ta_3N_5 electrodes as tabulated in Figure 5b, the smaller τ_2 of necked-Ta_3N_5 electrode means that necking treatment decrease the charge transfer resistance (R_{bulk}) in Ta_3N_5 film.

The amorphous layer of nitrogen doped tantalum oxide that bridges the Ta_3N_5 particles is plausible to pave the route for electron transportation. As necking treatment is performed at high temperature, efficient connection at interfaces of PP will be formed. Additionally, nitrogen doping in the tantalum oxide layer can improve its conductivity[48] and facilitate the transportation of the photogenrated charges. Indeed, it is reasonable that low charge transfer resistance should take responsibility for the high photovoltage and fast decay process since the Dember photovoltage is caused by drifting apart of electron-hole pairs, the better the conductivity is, the easier they can be dissociated/recombined, and vice versa.

The efficiency of electrons transportation across the interfaces of PP and PS was further probed using the benchmark redox couple of ferri/ferrocyanide.[23] The exchange of electrons between the solution and electrodes is fast (Figure S8 (a)), allowing for the characterization of electron transfer by CV. And the reduction reaction occurred on Ta_3N_5 electrode (without illumination) can provide direct views on the electron transportation. In darkness, the electrochemical reduction is

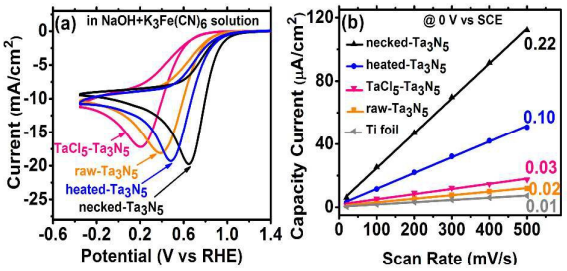

Figure 6. (a) Cyclic voltammograms on raw-Ta_3N_5 (orange), $TaCl_5$-Ta_3N_5 (pink), heated-Ta_3N_5 (blue), and necked-Ta_3N_5 (black) electrodes for the reduction of ferricyanide in NaOH+$K_3Fe(CN)_6$ aqueous solution. (b) The plots of capacitive current to scan rate for the Ti foil (grey), raw-Ta_3N_5 (orange), $TaCl_5$-Ta_3N_5 (pink), heated-Ta_3N_5 (blue), and necked-Ta_3N_5 (black) electrodes. The slopes are shown beside the curves.

occurred by transferring electrons from the Ta_3N_5 electrode to $K_3Fe(CN)_6$. Better electron transportation in the film will lead to more facial electron exchange. Moreover, the improved electron transfer in the film will decrease the Ohmic polarization of the electrode, hence, decrease the overpotential for the reduction of $K_3Fe(CN)_6$. The CV reveals that Ta_3N_5 is dull for hydrogen evolution (Figure S8 (b)) but preferred to $K_3Fe(CN)_6$ reduction (Figure S8 (c)). It allows us to focus on the electron exchange between electrode and $K_3Fe(CN)_6$ regardless of the influence of hydrogen evolution in the potential window of -0.4 V~1.2 V vs RHE. And in Figure S8 (c), it shows that the reduction peak of $K_3Fe(CN)_6$ shifts positively on Ta_3N_5 electrode, indicating that Ta_3N_5 is superior to the Ti substrate in electrocatalytic reduction of $K_3Fe(CN)_6$. When Ta_3N_5 film has a good (poor) contact with the substrate, more electron will be exchanged with $K_3Fe(CN)_6$ on the Ta_3N_5 particles (Ti substrate) (Figure S9). Thus, the results in Figure 6a can be related to the electron transfer in Ta_3N_5 film. It is found that the necked-Ta_3N_5 electrode has a reduction current of -19.7 mA/cm^2 at 0.65 V vs RHE, while that for the raw-Ta_3N_5 electrode is -18.1 mA/cm^2 at 0.38 V vs RHE, which is similar to that of the substrate (Figure S8 (c)). The more positive potential along with higher current of the reduction peak indicates more efficient electron exchange on necked-Ta_3N_5 electrode. Because electrons should transport through the particulate Ta_3N_5 film, it is concluded that necked-Ta_3N_5 electrode is superior to raw-Ta_3N_5 electrode in electron transportation (Figure S9). The reduction peak potential of raw-Ta_3N_5 electrode (0.38 V vs RHE) is close to the substrate (0.37 V vs RHE), indicating that more electrons are leaked out through the substrate other than Ta_3N_5 because of the weak connection at the PS interfaces. Additionally, the CV of CoPi/necked-Ta_3N_5 electrode is similar to that of necked-Ta_3N_5 electrode (Figure S8 (d)), confirming that CoPi has little impact on the charge transfer in the electrode.

To sum up, necking treatment can facilitate charge transfer at the PP and PS interfaces in the Ta_3N_5 film which is beneficial for the collection of photogenerated electrons, and depressing the recombination at the interfaces.

For particulate electrode, only the particles having good connection with the conductive layer can provide the area for electrochemical reaction. And if electrode made from powder has good conductivity in the film, porous structure with large electrochemical active area is expected. By eliminating the influence of diffusion layer with concentrated electrolyte, we can get the relative area of the electrode from its charging capacitance of the Helmholtz double layer based on the following expression:[8, 24]

$j=vC=(\varepsilon S/4\pi d)v$ (4)

Where v is the scan rate, C is the capacitance of the double layer which is proportional to the surface area S.

Here, we measured the charging current (j) in a potential window (-0.1 V~ 0.2 V vs SCE) where there is no Faradic current at different scan rates without illumination (Figure S10). The j-v plot of each electrode is shown in Figure 6b. And the slope should be proportional to the surface area based on eq. (4). Taking the area of bare Ti substrate as unit, it is found the area only increases a little with $TaCl_5$ treatment or heating. But the refined necking treatment leads to 22 times larger of the electrochemical surface area. Based on the analysis above, it is inferred that for raw-Ta_3N_5 electrode, the poor connection in the particulate Ta_3N_5 layer contributes little to the electrochemical active area. Only the layer of Ta_3N_5 contact with the substrate can be used for reaction (Figure S9, left). Thus the electrochemical area is limited. After necking treatment, the connection at the interfaces of particle-particle (PP) and particle-substrate (PS) are improved prominently and ever the layer of Ta_3N_5 far from the substrate can be used for reaction (Figure S9, right). So the necked-Ta_3N_5 electrode provides much larger electrochemical surface area for reaction.

Inspired by the results above, another example was further raised to support the conclusion. We found that the necking treatment can improve the photocurrent to 6.0 mA/cm^2 at 1.6 V vs RHE for the Ta_3N_5 electrodes made from traditional thermal oxidation-nitridation method (Figure S11, see ESI for detail).

As for the role of CoPi, it can improve the charge separation by enhancing the charge generation in the Ta_3N_5 crystal as shown *vide supra*. And the surface charge injection process is also greatly accelerated with CoPi (Figure S12). Because of the cocatalyst promoted charge separation and injection, the CoPi/necked-Ta_3N_5 electrode can provide a photocurrent of 11.2 mA/cm^2 at 1.6 V vs RHE. Moreover, the fast consuming of photogenerated holes can protect Ta_3N_5 from being oxidized.[44] Thus, the stability of necked-Ta_3N_5 electrode are prominently improved with the assistance of CoPi as shown in Figure 7a. The near unit Faradic efficiency of CoPi/necked-Ta_3N_5 electrode (Figure 7b) confirms that the photocurrent is originated from O_2 evolution reaction. However, the photocurrent decayed noticeably with prolonging time (Figure 7a). The failure of the Ta_3N_5 electrode is suspected to be the result of large surface area of the particulate electrode which makes it difficult to wholly cover Ta_3N_5 with effective co-catalyst in the porous structure. Many unconsumed photogenerated holes were accumulated and destroyed the intrinsic Ta_3N_5. Further endeavours of improving the stability is still in progress.

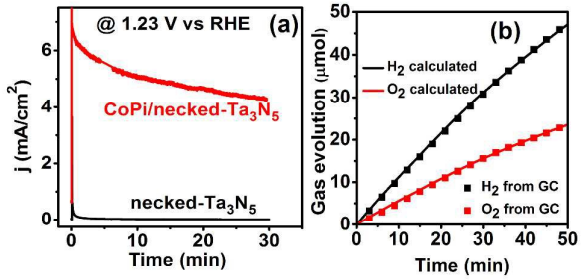

Figure 7. (a) Stability of the necked-Ta_3N_5 (black) and CoPi/necked-Ta_3N_5 (red) photoanodes at 1.23 V vs RHE. (b) Faradaic efficiency of the CoPi/necked-Ta_3N_5 photoanode at 1.23 V vs RHE. Electrolyte: 1 M NaOH aqueous solution. Illumination: 100 mW/cm^2, Xe lamp (Wavelength >420 nm). Area: 0.6 cm^2.

Conclusions

Efficient Ta_3N_5 photoanode is fabricated on Ti foil by EPD method with refined necking treatment. Further loading cocatalyst of CoPi gives a photocurrent of 6.1 mA/cm^2 at 1.23 V vs RHE under simulated sunlight (AM 1.5G). To the best of our knowledge, it is the highest photoresponse for electrode made by EPD. The benefit of necking treatment is proved to stem from the high temperature treatment and the formation of nitrogen doped tantalum oxide layer, which can improve the charge separation efficiency. The TPV shows higher Dember photovoltage and faster decay process for necked-Ta_3N_5 electrode, which suggests that necking treatment can decrease the charge transfer resistance at the interfaces of particle-particle. It will promote the collection of photogenerated charges, decrease the recombination at the interfaces and improve the charge separation efficiency. Following CV measurement further confirms the benefit of necking treatment in promoting electron transfer and providing more electrochemically active area for surface water oxidation.

Acknowledgements

This work was supported by the Basic Research Program of China (973 Program: 2014CB239403), and Natural Science Foundation of China (No. 21522306, 21373210).

Notes and references

1 N. Getoff, International Journal of Hydrogen Energy, 1990, **15**, 407-417.
2 X. Chen, S. Shen, L. Guo and S. S. Mao, *Chemical Reviews*, 2010, **110**, 6503-6570.
3 Z. Chen, T. F. Jaramillo, T. G. Deutsch, A. Kleiman-Shwarsctein, A. J. Forman, N. Gaillard, R. Garland, K.

Takanabe, C. Heske and M. Sunkara, *J. Mater. Res*, 2010, **25**, 3.
4 D. Kang, T. W. Kim, S. R. Kubota, A. C. Cardiel, H. G. Cha and K. S. Choi, *Chemical Reviews*, 2015.
5 K. Maeda, T. Takata, M. Hara, N. Saito, Y. Inoue, H. Kobayashi and K. Domen, *Journal of the American Chemical Society*, 2005, **127**, 8286-8287.
6 S. Chen, J. Yang, C. Ding, R. Li, S. Jing, D. Wang, H. Han, F. Zhang and C. Li, *Journal of Materials Chemistry A*, 2013, **1**, 5651-5659.
7 X. Wang, Q. Xu, M. Li, S. Shen, X. Wang, Y. Wang, Z. Feng, J. Shi, H. Han and C. Li, *Angewandte Chemie International Edition*, 2012, **51**, 13089-13092.
8 B. A. Pinaud, P. C. Vesborg and T. F. Jaramillo, *The Journal of Physical Chemistry C*, 2012, **116**, 15918-15924.
9 Y. Ling, G. Wang, D. A. Wheeler, J. Z. Zhang and Y. Li, *Nano Letters*, 2011, **11**, 2119-2125.
10 Z. Wang, G. Liu, C. Ding, Z. Chen, F. Zhang, J. Shi and C. Li, *The Journal of Physical Chemistry C*, 2015, **119**, 19607-19612.
11 S. D. Tilley, M. Cornuz, K. Sivula and M. Grätzel, *Angewandte Chemie*, 2010, **122**, 6549-6552.
12 L. Zhang, T. Minegishi, J. Kubota and K. Domen, *Physical Chemistry Chemical Physics*, 2014, **16**, 6167-6174.
13 C. Zhen, T. Wu, M. W. Kadi, I. Ismail, G. Liu and H.-M. Cheng, *Chinese Journal of Catalysis*, 2015, **36**, 2171-2177.
14 Y. Li, L. Zhang, A. Torres-Pardo, J. M. González-Calbet, Y. Ma, P. Oleynikov, O. Terasaki, S. Asahina, M. Shima and D. Cha, *Nature communications*, 2013, **4**.
15 Y. Qiu, S.-F. Leung, Q. Zhang, B. Hua, Q. Lin, Z. Wei, K.-H. Tsui, Y. Zhang, S. Yang and Z. Fan, *Nano Letters*, 2014, **14**, 2123-2129.
16 M. Stefik, M. Cornuz, N. Mathews, T. Hisatomi, S. Mhaisalkar and M. Grätzel, *Nano Letters*, 2012, **12**, 5431-5435.
17 S. R. Pendlebury, M. Barroso, A. J. Cowan, K. Sivula, J. Tang, M. Grätzel, D. Klug and J. R. Durrant, *Chemical Communications*, 2011, **47**, 716-718.
18 Y. Tamaki, A. Furube, M. Murai, K. Hara, R. Katoh and M. Tachiya, *Physical Chemistry Chemical Physics*, 2007, **9**, 1453-1460.
19 Y. Ma, S. R. Pendlebury, A. Reynal, F. Le Formal and J. R. Durrant, *Chemical Science*, 2014, **5**, 2964-2973.
20 R. Esposito, J. Loferski and H. Flicker, *Journal of applied physics*, 1967, **38**, 825-831.
21 R. Wilson, Critical Reviews in Solid State and Material Sciences, 1980, **10**, 1-41.
22 L. M. Peter, *Chemical Reviews*, 1990, **90**, 753-769.
23 Y. W. Chen, J. D. Prange, S. Dühnen, Y. Park, M. Gunji, C. E. Chidsey and P. C. McIntyre, *Nature Materials*, 2011, **10**, 539-544.
24 A. J. Bard and L. R. Faulkner, *Electrochemical methods: fundamentals and applications*, Wiley New York, 1980.
25 M. de Respinis, M. Fravventura, F. F. Abdi, H. Schreuders, T. J. Savenije, W. A. Smith, B. Dam and R. van de Krol, *Chemistry of Materials*, 2015, **27**, 7091-7099.
26 S. Chen, S. Shen, G. Liu, Y. Qi, F. Zhang and C. Li, *Angewandte Chemie International Edition*, 2015, **54**, 3047-3051.
27 P. Zhang, J. Zhang and J. Gong, *Chemical Society Reviews*, 2014, **43**, 4395-4422.
28 X. Zong, S. Thaweesak, H. Xu, Z. Xing, J. Zou, G. M. Lu and L. Wang, *Physical Chemistry Chemical Physics*, 2013, **15**, 12314-12321.
29 D. Wang, R. Li, J. Zhu, J. Shi, J. Han, X. Zong and C. Li, *The Journal of Physical Chemistry C*, 2012, **116**, 5082-5089.
30 M. Liao, J. Feng, W. Luo, Z. Wang, J. Zhang, Z. Li, T. Yu and Z. Zou, *Advanced Functional Materials*, 2012, **22**, 3066-3074.
31 R. Abe, M. Higashi and K. Domen, *Journal of the American Chemical Society*, 2010, **132**, 11828-11829.
32 M. Higashi, K. Domen and R. Abe, *Journal of the American Chemical Society*, 2012, **134**, 6968-6971.
33 S. S. Gujral, A. N. Simonov, X.-Y. Fang, M. Higashi, T. Gengenbach, R. Abe and L. Spiccia, *Catalysis Science & Technology*, 2016.
34 M. Higashi, K. Domen and R. Abe, *Journal of the American Chemical Society*, 2013, **135**, 10238-10241.
35 M. Hara, E. Chiba, A. Ishikawa, T. Takata, J. N. Kondo and K. Domen, *The Journal of Physical Chemistry B*, 2003, **107**, 13441-13445.
36 A. Arranz and C. Palacio, *Applied Physics A*, 2005, **81**, 1405-1410.
37 D. Yokoyama, H. Hashiguchi, K. Maeda, T. Minegishi, T. Takata, R. Abe, J. Kubota and K. Domen, *Thin Solid Films*, 2011, **519**, 2087-2092.
38 A. Ibidunni, R. MaSaitis, R. Opila, A. Davenport, H. Isaacs and J. Taylor, *Surface and Interface Analysis*, 1993, **20**, 559-564.
39 M. W. Kanan, Y. Surendranath and D. G. Nocera, *Chemical Society Reviews*, 2009, **38**, 109-114.
40 M. Higashi, K. Domen and R. Abe, *Energy & Environmental Science*, 2011, **4**, 4138-4147.
41 J. Feng, W. Luo, T. Fang, H. Lv, Z. Wang, J. Gao, W. Liu, T. Yu, Z. Li and Z. Zou, *Advanced Functional Materials*, 2014, **24**, 3535-3542.
42 J. Yang, D. Wang, H. Han and C. Li, *Accounts of Chemical Research*, 2013, **46**, 1900-1909.
43 H. Dotan, K. Sivula, M. Grätzel, A. Rothschild and S. C. Warren, *Energy & Environmental Science*, 2011, **4**, 958-964.
44 G. Liu, J. Shi, F. Zhang, Z. Chen, J. Han, C. Ding, S. Chen, Z. Wang, H. Han and C. Li, *Angewandte Chemie*, 2014.
45 B. C. O'Regan, K. Bakker, J. Kroeze, H. Smit, P. Sommeling and J. R. Durrant, *The Journal of Physical Chemistry B*, 2006, **110**, 17155-17160.
46 M. Barroso, A. J. Cowan, S. R. Pendlebury, M. Grätzel, D. R. Klug and J. R. Durrant, *Journal of the American Chemical Society*, 2011, **133**, 14868-14871.
47 F. Fabregat-Santiago, G. Garcia-Belmonte, J. Bisquert, A. Zaban and P. Salvador, *The Journal of Physical Chemistry B*, 2002, **106**, 334-339.
48 H. Nie, S. Xu, S. Wang, L. You, Z. Yang, C. Ong, J. Li and T. Liew, *Applied Physics A*, 2001, **73**, 229-236.